Supplementary material (ESI) for Journal of Materials Chemistry

Supplementary Information

This section consists of two parts: Experimental Methods and Characterization

Experimental Methods

1,2-bis(10,12-tricosadiynoyl)-*sn*-glycero-3-phosphocholine ($DC_{8,9}PC$) was purchased from Avanti Polar Lipids, Inc. Ammonium iron (II) sulfate hexhydrate ($(NH_4)_2Fe(SO_4)_2{\cdot}6H_2O$), and hydrogen peroxide (H_2O_2) (30 wt. % in water) were purchased from Aldrich Chemical Co. A schematic diagram illustrating the formation of nanotubes containing inorganic layers is shown in Figure 1. Initially, $DC_{8,9}PC$ nanotubes were obtained using the literature method.[1] 10 mL of an aqueous dispersion with 1.1 mol/L $DC_{8,9}PC$ nanotubes was purged with N_2 for 0.5 hr, followed by the addition of 0.5 mL of 0.4 mol/L ammonium iron (II) sulfate hexhydrate aqueous solution, which served as a reducing agent. After 0.5 hr, the final step involved the addition of 0.2 mmol of hydrogen peroxide, which acted as an oxidizing agent to react with the reducing agent. The reaction continued for 1 hour after which time the product was collected by centrifuging and dialysis to remove excess ions. Due to the presence of Fe^{3+} oxidized from Fe^{2+} by H_2O_2 the final nanotube product exhibited a light yellow color. Finally, nanotubes were freeze dried and annealed at 550 °C for 0.5 hour.

Morphologies of nanotubes were analyzed using a Jeol JEM-2100 transmission electron microscope (TEM) operated at 200 kV, in which samples were diluted and deposited on formvar/carbon coated copper grids. Magnetic hysteresis measurements were performed using a MicroMag Model 2900 alternating gradient magnetometer (AGM, Princeton Measurement Corp.) at room temperature. Raman spectra and images were obtained with a Renishaw inVia Raman microscope equipped with a computer-controlled three-axis

encoded (XYZ) motorized stage, a RenCam CCD detector, and a Leica microscope (DMLM series). The 785 nm diode laser provided Raman excitation with a maximum power output of 300 mW. The sample solutions were deposited on the gold surface and allowed to dry overnight. The Raman spectra of samples were collected with a 30 mW laser power on the sample and an acquisition time of 30 sec. Raman images were obtained with the dielectric tunable filter band-pass centered at 1508 cm^{-1} using an acquisition time of 2 min and a ×100 objective.

Characterization

In order to follow chemical changes resulting from Steps 1, 2, and 3, Raman analysis was performed. Traces A, B, and C of Figure S-1 illustrate a series of Raman spectra recorded after each step in Figure 1. Trace A, collected from Step 1, illustrates the Raman spectrum of $DC_{8,9}PC$ nanotubes, which exhibit C≡C stretching vibrations manifested by the band at 2259 cm^{-1}. As shown in Trace B, Raman spectrum recorded after Step 2 exhibits the presence of the band at 1610 cm^{-1} due to H_2O stretching vibrations, the band at 1021 cm^{-1} due to SO_4^{2-} stretching vibrations, and the 602 cm^{-1} band resulting from the Fe-O vibrations. It should be noted that after Step 2 nanotubes contains H_2O, SO_4^{2-}, and Fe-O species. Based on the literature data, there are two types of structures which contain these species: iron (III) oxyhydroxy sulfate $(Fe_8O_8(OH)_x(SO_4)_y)$[2] and amorphous basic iron (III) sulfate $(2Fe_2O_3 \cdot SO_3 \cdot xH_2O)$.[3] Since the bands due to –OH vibrations are present in iron (III) oxyhydroxy sulfate, which is absent after Step 2, iron (III) oxyhydroxy sulfate is unlikely to be present. In contrast, amorphous basic iron (III) sulfate prepared from hydrolytic precipitation of the $Fe_2(SO_4)_3$ solution at pH 5-6 matches our

spectroscopic data. Thus, chemical composition after Step 2 is believed to be amorphous basic iron (III) sulfate.[3] As seen in Trace B (Step 2), the band at 2259 cm^{-1} due to C≡C stretching vibrations exhibits lower intensity, and new bands detected at 2109 cm^{-1} and 1508 cm^{-1} are due to C≡C and C=C stretching vibrations of polymerized interlayer structures, respectively.[4] The latter result from polymerization of diacetylenic groups of $DC_{8,9}PC$ which is initiated by the radicals generated by Fe^{2+}/H_2O_2 redox reactions, and the formation of alternating C≡C and C=C conjugated structures. As seen in Trace C recorded after Step 3, the bands at 226, 293, 412, 500, 615, and 658 cm^{-1} are detected, which is in agreement with the reported Raman spectrum of hematite (α-Fe_2O_3).[5-7] In addition, two bands at 1595 and 1329 cm^{-1} are observed which are attributed to the tangential G-band resulting from the graphite-like in plane mode and the disorder-induced D-band of carbon nanotubes, respectively. However, the presence of dopants is not detected.

In an attempt to combine morphological and chemical information, an optical microscopic image (insert D of Figure S-1) and Raman imaging of a nanotube after Step 2 (insert E of Figure S-1) are shown. While the optical image manifests the tubular morphology, Raman image of the same nanotube was collected by tuning into the C=C band at 1508 cm^{-1}. Again, tubular morphology is clearly observed, where green area represents the 1508 cm^{-1} band intensity.

The selected area electron diffraction (SAD) pattern for FMNTs is shown in Figure S-2, A. For comparison, the SAD for hematite (α-Fe_2O_3) is shown in Figure S-2, B. Using these data we determined the d-spacing values for both specimens which are summarized in Table S-1. Typical d-spacing values observed for hematite at 012, 110, 300 are not

detected for FMNTs, but the additional 013 reflection is present, which might be attributed to the presence of other iron oxide phases, especially in the presence of S, C, N, and P elements in the FMNTs domains as well as concentric morphologies. Determination of crystallographic structures responsible for magnetization is the focus of the ongoing investigation.

Supplementary material (ESI) for Journal of Materials Chemistry

References

1 P. Yager and P. E. Schoen, *Mol. Cryst. Liq. Cryst.*, 1984, **106**, 371.
2 U. Schwertmann and R. M. Cornell, 'Iron Oxides in the Laboratory: Preparation and Characterization ', Weinheim, 2000.
3 E. V. Margulis, L. A. Savchenko, M. M. Shokarev, L. I. Beisekeeva, and F. I. Vershinina, *Russ. J. Inorg. Chem*, 1975, **20**, 1045.
4 P. E. Schoen and P. Yager, *J. Polym. Sci. Polym. Phys. Ed.*, 1985, **23**, 2203.
5 D. Bersani, P. P. Lottici, and A. Montenero, *J. Raman Spectrosc.*, 1999, **30**, 355.
6 H. Q. Cao, G. Z. Wang, L. Zhang, Y. Liang, S. C. Zhang, and X. R. Zhang, *Chem. Phys. Chem.*, 2006, **7**, 1897.
7 K. F. McCarty, *Solid State Commun.*, 1988, **68**, 799.

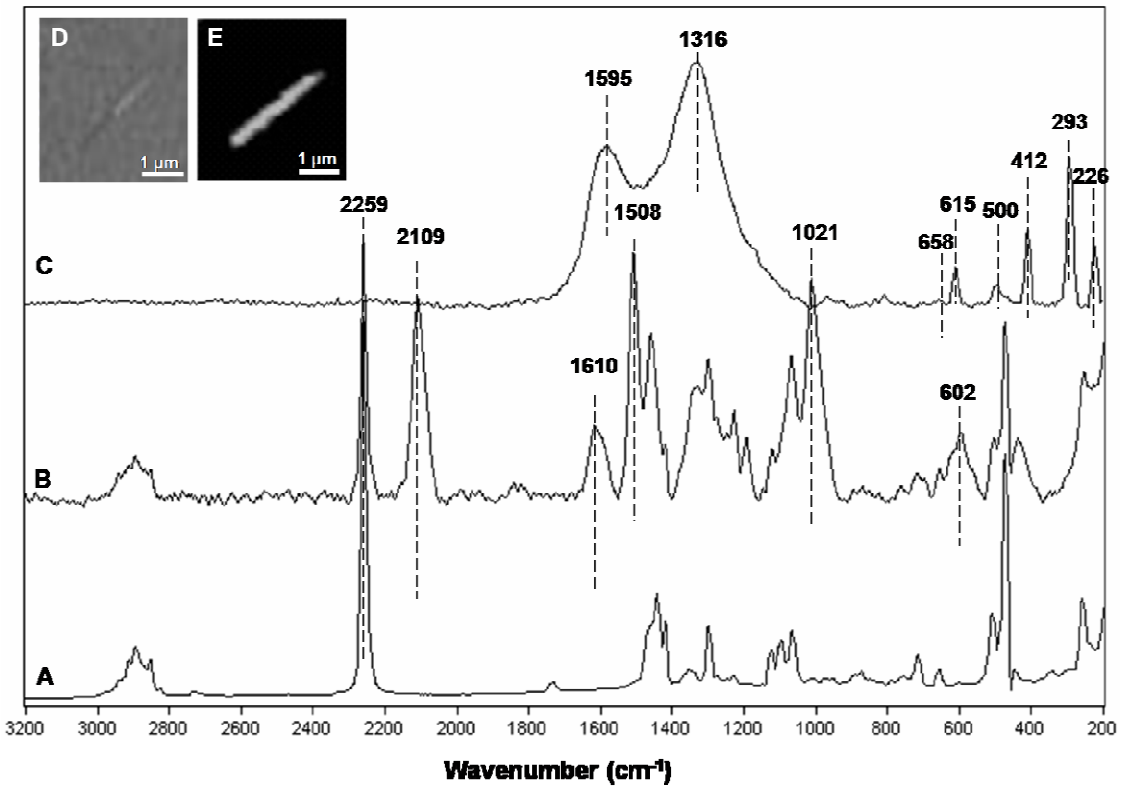

Figure S-1. Raman spectra in the 3200-200 cm^{-1} region of nanotubes after Step 1 (A), Step 2 (B), and Step 3 (C). Optical image (D) and Raman image (E) of nanotubes after Step 2.

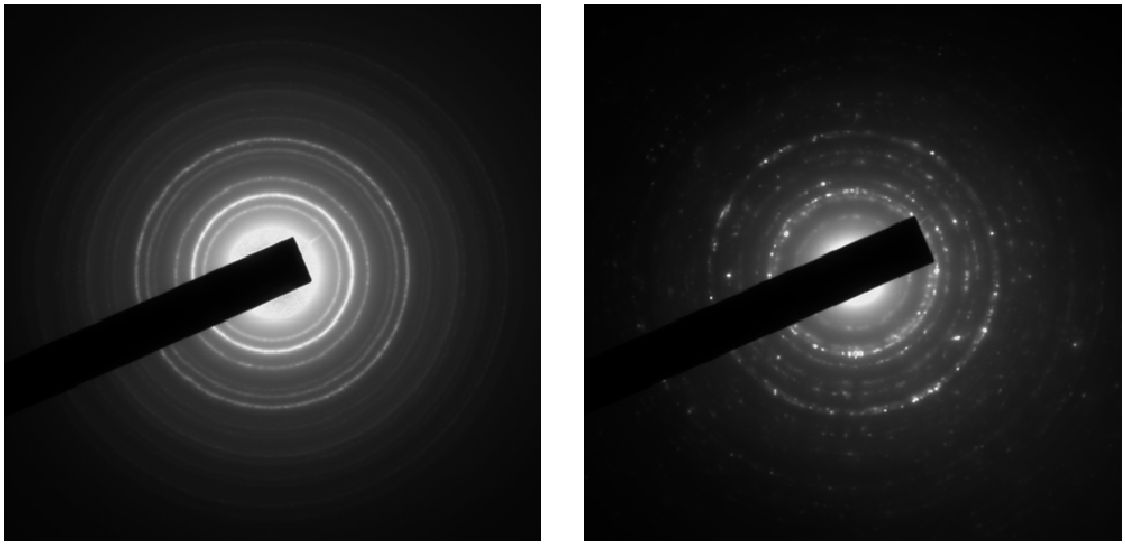

Figure S-2. Selected area electron diffraction (SAD) images of FMNT (A) and hematite (B).

Supplementary material (ESI) for Journal of Materials Chemistry

Table S-1. Calculated d-spacings of FMNT and hematite from Figure S-2.

FMNT d-spacing (Å)	Hematite d-spacing (Å)	Hematite (hkl)
—	3.68	012
3.19	—	013
2.73	2.70	104
—	2.52	110
2.23	2.21	113
1.84	1.84	024
1.73	1.69	116
1.60	1.61	122
—	1.49	300